

Learning to Select Like Humans: Explainable Active Learning for Medical Imaging

Ifrat Ikhtear Uddin¹, Longwei Wang¹, Xiao Qin², Yang Zhou² and KC Santosh¹

Abstract—Medical image analysis requires substantial labeled data for model training, yet expert annotation is expensive and time-consuming. Active learning (AL) addresses this challenge by strategically selecting the most informative samples for the annotation purpose, but traditional methods solely rely on predictive uncertainty while ignoring whether models learn from clinically meaningful features a critical requirement for clinical deployment. We propose an explainability-guided active learning framework that integrates spatial attention alignment into a sample acquisition process. Our approach advocates for a dual-criterion selection strategy combining: (i) classification uncertainty to identify informative examples, and (ii) attention misalignment with radiologist-defined regions-of-interest (ROIs) to target samples where the model focuses on incorrect features. By measuring misalignment between Grad-CAM attention maps and expert annotations using *Dice similarity*, our acquisition function judiciously identifies samples that enhance both predictive performance and spatial interpretability. We evaluate the framework using three expert-annotated medical imaging datasets, namely, BraTS (MRI brain tumors), VinDr-CXR (chest X-rays), and SIIM-COVID-19 (chest X-rays). Using only 570 strategically selected samples, our explainability-guided approach consistently outperforms random sampling across all the datasets, achieving 77.22% accuracy on BraTS, 52.37% on VinDr-CXR, and 52.66% on SIIM-COVID. Grad-CAM visualizations confirm that the models trained by our dual-criterion selection focus on diagnostically relevant regions, demonstrating that incorporating explanation guidance into sample acquisition yields superior data efficiency while maintaining clinical interpretability.

I. INTRODUCTION

Deep learning has achieved remarkable progress in medical image analysis, enabling automated detection and classification across diverse imaging modalities including MRI, CT, and chest X-ray [1], [2], [3]. However, these advances rely heavily on large-scale annotated datasets a scarce resource in clinical domains where expert labeling is time consuming, expensive, and requires specialized medical knowledge. The fundamental challenge is achieving strong model performance while minimizing the number of labeled samples required the core objective of data-efficient learning [4], [5].

Active learning (AL) addresses this data efficiency challenge by intelligently selecting which samples should be labeled, thereby maximizing model improvement per annotation [6], [7]. Traditional AL methods for deep learning rely primarily on uncertainty-based selection criteria such as

¹Ifrat Ikhtear Uddin, Longwei Wang, KC Santosh are with AI Research, Department of Computer Science, University of South Dakota, Vermillion, SD 57069, USA ifratikhtear.uddin@coyotes.usd.edu, longwei.wang@usd.edu, [kc.santosh@usd.edu](mailto:kcsantosh@usd.edu)

²Xiao Qin and Yang Zhou with Department of Computer Science and Software Engineering, Auburn University, Auburn, AL 36849, USA xqin@auburn.edu, yangzhou@auburn.edu

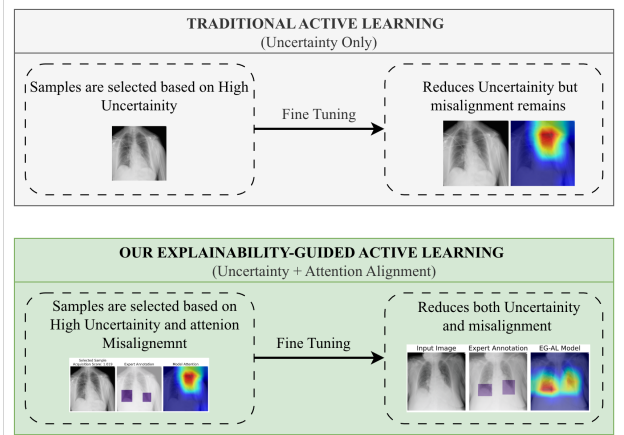


Fig. 1. Traditional AL only considers uncertainty. It misses samples where the model is confident but focuses on the wrong features. Our dual-criterion approach catches both failure modes

entropy [8] or model disagreement. These approaches operate on a single principle: select samples where the model is most uncertain, under the assumption that reducing classification error is sufficient for building robust models.

However, this single-criterion approach has a critical limitation in medical imaging: uncertainty alone cannot distinguish between samples that are informative for the right reasons versus the wrong reasons. Consider two scenarios: (1) a sample where the model is uncertain but already attends to the correct diagnostic region, and (2) a sample where the model is confident but focuses on spurious features like image artifacts or background patterns. Traditional uncertainty-based AL would prioritize the first sample while potentially ignoring the second yet from a clinical deployment perspective, the second sample is arguably more valuable because it reveals and can correct fundamental flaws in the model’s decision-making process.

This limitation is particularly problematic in high-stakes medical applications where model interpretability is not optional but required for clinical trust, regulatory approval, and patient safety [9], [10], [11]. A model that achieves high accuracy while attending to anatomically irrelevant regions is unsuitable for deployment, regardless of its performance metrics. Neural networks are known to exploit dataset biases and shortcuts [12], and uncertainty-based selection provides no mechanism to detect or correct such behavior during the sample acquisition process.

Explainable AI (XAI) methods such as Grad-CAM [13] and SHAP [14] provide post-hoc visualizations of model at-

tention, revealing which image regions influence predictions. Recent work has incorporated explanation guidance into model *training* [15], [16], [17], [18], [19], using radiologist-annotated regions-of-interest (ROIs) to supervise attention and improve spatial alignment. However, these approaches focus on how to train with available data, not which data to select. A critical question remains unanswered: **can explanation quality specifically, attention alignment with expert annotations guide sample selection to improve data efficiency beyond what uncertainty alone achieves?**

We hypothesize that effective sample selection requires dual-criterion reasoning that jointly considers: **What the model doesn't know** (high uncertainty) samples at decision boundaries that refine classification; **What the model knows incorrectly** (attention misalignment) samples where the model focuses on wrong features despite potentially high confidence. These criteria are complementary: uncertainty identifies samples that challenge the model's predictions, while explanation misalignment identifies samples that reveal flawed reasoning. By combining both as shown in Fig. 1, we can systematically select samples that improve not only accuracy but also the *quality* of decision making, ensuring models learn from diagnostically relevant features rather than shortcuts.

To solve this problem, we propose an **Explainability-Guided Active Learning (EG-AL)** framework that integrates spatial attention alignment into sample acquisition. Our approach introduces a composite scoring function that balances classification entropy (uncertainty) with Grad-CAM-based attention misalignment measured via Dice similarity against expert ROIs. This dual-criterion selection enables us to identify samples that traditional uncertainty-only methods would miss: cases where the model exhibits correct confidence levels but incorrect attention patterns, or vice versa. Our main contributions are:

- 1) We introduce an explainability-guided active learning framework that combines classification uncertainty with spatial attention alignment for sample selection. Unlike traditional uncertainty-only methods, our dual-criterion approach explicitly measures attention-ROI misalignment to identify samples that improve both predictive accuracy and clinical interpretability.
- 2) We propose a principled acquisition function that balances entropy-based uncertainty with Grad-CAM ROI misalignment quantified via Dice similarity. This enables systematic identification of samples where models exhibit correct uncertainty but incorrect attention, or vice versa distinctions that single-criterion methods cannot capture.
- 3) We demonstrate substantial gains in data efficiency across three medical imaging datasets and two modalities (MRI, X-ray), achieving consistent improvements over random sampling with only 570 samples. Our results validate that incorporating explanation quality into sample acquisition yields superior performance per labeled sample, establishing a new paradigm for data-efficient medical AI that jointly optimizes accuracy and interpretability.

racy and interpretability.

II. RELATED WORK

A. AL for Annotation Efficiency

AL has long been recognized as an effective strategy for reducing annotation burdens by selectively querying the most informative unlabeled samples for labeling [20], [21], [22]. In medical imaging, AL is especially useful due to the high cost and limited availability of expert annotators [23], [24]. Recent methods such as ACFT (Active, Continual Fine-Tuning) [25], [26] have successfully integrated active sampling into deep learning workflows. ACFT employs entropy and diversity-based acquisition functions to select diverse and uncertain samples across multiple clinical tasks, including colonoscopy frame classification and pulmonary embolism detection. Similarly, Hao et al. [27] combined uncertainty sampling with a query-by-committee strategy to construct a transfer learning-based AL pipeline for brain tumor classification.

While these methods significantly reduce labeling costs and improve generalization, they primarily rely on uncertainty estimation through softmax probabilities or ensemble disagreement, which are known to be overconfident and unreliable in deep models [8]. Moreover, these acquisition strategies do not incorporate any measure of model interpretability or alignment with domain knowledge, thereby limiting their usefulness in high-stakes clinical settings where human oversight and trust are essential.

B. Explainable AI in Medical Imaging

Explainable Artificial Intelligence (XAI) has become a critical focus in medical AI to ensure that model decisions are transparent, justifiable, and aligned with human expert reasoning [28], [29], [30], [31]. Among the most popular post-hoc explanation methods are Grad-CAM [13] and SHAP [14], which visualize salient regions of input images that contribute to model predictions. These methods have been extensively applied in medical tasks such as diabetic retinopathy detection, chest X-ray diagnosis, and brain tumor segmentation [32], [33], [34], [35].

However, a key limitation of most XAI techniques is that they are applied after model training, meaning they do not influence the model's learning trajectory. As a result, models may still rely on spurious or non-causal features during inference, even if their explanations appear visually plausible. This disconnect between training and interpretation reduces the clinical reliability of post-hoc explanations and undermines efforts to build transparent AI systems.

C. Explainability-Guided Sample Selection in Active Learning

While recent works have demonstrated the value of integrating explanation guidance into model training [15], [16], [17], these approaches focus primarily on improving spatial attention during the learning process rather than leveraging explainability to inform which samples should be acquired.

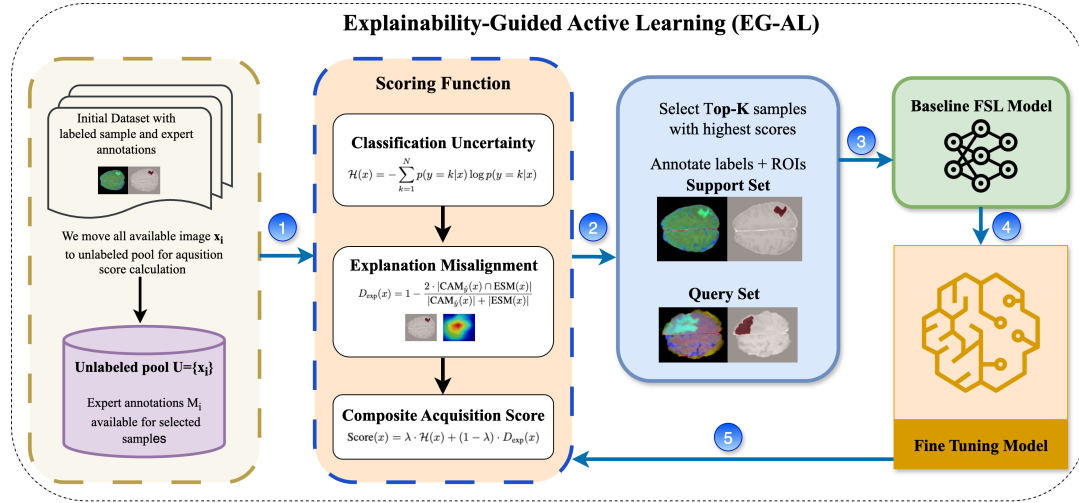


Fig. 2. Explainability-Guided Active Learning Framework. The framework operates in an iterative cycle with five key components: (1) Starting with an unlabeled pool $U = \{x_i\}$ where expert annotations are available for selected samples; (2) A composite scoring function that combines classification uncertainty $H(x)$ and explanation misalignment $D_{exp}(x)$; (3) Selection of top-K samples with highest composite scores, followed by expert annotation to obtain both class labels and diagnostic ROI masks for support and query sets; (4) Model fine-tuning with explanation-guided supervision using the newly acquired expert annotations. This iterative system progressively improves both classification accuracy and explanation quality while minimizing annotation costs.

For instance, Šefčík et al. [15] used Layer-wise Relevance Propagation (LRP) to guide model attention towards glioma tumor regions in brain MRI, while Caragliano et al. [16] incorporated radiologist-annotated regions-of-interest (ROIs) to supervise attention in lung cancer CT imaging. These methods enhance interpretability through explanation-supervised training.

Traditional active learning strategies prioritize samples based on predictive uncertainty or diversity metrics, operating under the assumption that reducing classification error alone will yield clinically reliable models. However, these approaches overlook whether the model is learning from the correct features a sample may have high uncertainty but exhibit correct attention patterns, or conversely, high confidence with attention focused on spurious correlations. This gap is particularly problematic in medical imaging, where model decisions must align with diagnostic reasoning to ensure clinical trust and safety.

While recent works have demonstrated the value of integrating explanation guidance into model training [15], [16], [17], [36], these approaches focus primarily on improving spatial attention during the learning process rather than leveraging explainability to inform which samples should be acquired. Traditional active learning strategies prioritize samples based on predictive uncertainty or diversity metrics, but do not incorporate measures of model interpretability or alignment with domain knowledge. This creates a critical gap: sample selection methods that optimize for predictive performance alone may inadvertently select data that reinforces spurious correlations rather than clinically meaningful features. Our work addresses this gap by introducing a dual-criterion acquisition function that combines classification uncertainty with spatial attention alignment, ensuring that selected samples improve both accuracy and clinical inter-

pretability.

III. METHODOLOGY

A. Explainable Active Learning

We present an explainability-guided active learning framework that strategically selects training samples by combining classification uncertainty with spatial attention alignment. Figure 2 illustrates our approach, which iteratively scores unlabeled samples using both predictive confidence and attention alignment between model attention (Grad-CAM) and expert annotations, then retrains with selected samples to progressively improve both accuracy and interpretability.

B. Problem Formulation

We consider a classification task with N classes and a pool of unlabeled images $\mathcal{U} = \{x_i\}_{i=1}^M$. Each image has an associated but unavailable label $y_i \in \{1, \dots, N\}$ and expert-provided spatial annotation $ESM(x_i)$ that indicates diagnostically relevant regions (e.g., tumor masks in BraTS, bounding boxes in VinDr-CXR and SIIM-COVID). Starting with a small labeled seed set \mathcal{S}_0 , our goal is to iteratively select batches of samples from \mathcal{U} that, when added to \mathcal{S} and used for model retraining, maximize both classification accuracy and spatial interpretability with minimal total annotations.

Our key insight is that effective sample selection requires jointly optimizing for both **what the model doesn't know** (uncertainty) and **what the model knows incorrectly** (attention misalignment).

C. Explainability-Guided Active Learning Framework

Figure 2 illustrates our EG-AL framework, which operates through an iterative cycle of scoring, selection, annotation, and retraining. At each iteration t :

- 1) **Scoring:** For each unlabeled sample $x \in \mathcal{U}$, compute a composite acquisition score combining classification uncertainty and explanation misalignment.
- 2) **Selection:** Select the top- K samples with highest scores to form batch \mathcal{B}_t .
- 3) **Annotation:** Retrieve ground-truth labels and spatial annotations for selected samples.
- 4) **Retraining:** Add \mathcal{B}_t to labeled set \mathcal{S}_t and retrain the model.
- 5) **Update:** Remove \mathcal{B}_t from \mathcal{U} and repeat.

The critical innovation lies in the scoring mechanism, which we describe in detail below.

D. Dual-Criterion Acquisition Function

For each unlabeled sample $x \in \mathcal{U}$, we compute an acquisition score that balances two complementary objectives:

- 1) **Classification Uncertainty:** We quantify predictive uncertainty using Shannon entropy over the model’s output distribution:

$$\mathcal{H}(x) = - \sum_{k=1}^N p(y = k|x) \log p(y = k|x), \quad (1)$$

where $p(y = k|x)$ denotes the predicted probability for class k . High entropy indicates samples near decision boundaries where the model is uncertain, making them informative for refining class separations.

2) **Explanation Misalignment:** To quantify whether the model attends to clinically relevant features, we compare model-generated attention maps against expert annotations. We use Grad-CAM [13] to generate a class activation map $\text{CAM}_{\hat{y}}(x)$ for the predicted class $\hat{y} = \arg \max_k p(y = k|x)$. This heatmap highlights spatial regions most influential for the model’s prediction.

We then measure the alignment between $\text{CAM}_{\hat{y}}(x)$ and the expert spatial annotation $\text{ESM}(x)$ using Dice similarity. The explanation misalignment score is defined as:

$$D_{\text{exp}}(x) = 1 - \frac{2 \cdot |\text{CAM}_{\hat{y}}(x) \cap \text{ESM}(x)|}{|\text{CAM}_{\hat{y}}(x)| + |\text{ESM}(x)|}, \quad (2)$$

where $|\cdot|$ denotes the sum of pixel values (for normalized heatmaps) or cardinality (for binary masks), and \cap represents element-wise multiplication. A high $D_{\text{exp}}(x)$ indicates that the model’s attention diverges significantly from expert expectations, revealing samples where the model relies on incorrect features.

3) **Composite Acquisition Score:** We combine both criteria into a unified acquisition score:

$$\text{Score}(x) = \lambda \cdot \mathcal{H}(x) + (1 - \lambda) \cdot D_{\text{exp}}(x), \quad (3)$$

where $\lambda \in [0, 1]$ controls the trade-off between uncertainty and misalignment. Setting $\lambda = 1$ reduces to pure uncertainty sampling (traditional AL), while $\lambda = 0$ selects only based on attention misalignment. Our experiments show that $\lambda = 0.5$ achieves strong performance across datasets, though it can be tuned for task-specific priorities.

This composite score enables us to identify samples that satisfy one of three informative patterns:

Algorithm 1 Explainability-Guided Active Learning

Require: Unlabeled pool \mathcal{U} , initial labeled set \mathcal{S}_0 , batch size K , balancing parameter λ , number of iterations T

- 1: Train initial model f_{θ_0} on \mathcal{S}_0
- 2: **for** $t = 1$ to T **do**
- 3: **for** each $x \in \mathcal{U}$ **do**
- 4: Forward pass: $p(y|x) = f_{\theta_{t-1}}(x)$
- 5: Compute uncertainty: $\mathcal{H}(x)$ using Eq. (1)
- 6: Generate Grad-CAM: $\text{CAM}_{\hat{y}}(x)$
- 7: Compute misalignment: $D_{\text{exp}}(x)$ using Eq. (2)
- 8: Compute score: using Eq 3
- 9: **end for**
- 10: Select batch: $\mathcal{B}_t \leftarrow \text{TopK}_{x \in \mathcal{U}}(\text{Score}(x))$
- 11: Retrieve labels and annotations for \mathcal{B}_t
- 12: Update labeled set: $\mathcal{S}_t \leftarrow \mathcal{S}_{t-1} \cup \mathcal{B}_t$
- 13: Retrain model: f_{θ_t} on \mathcal{S}_t using $\mathcal{L}_{\text{total}}$
- 14: Update pool: $\mathcal{U} \leftarrow \mathcal{U} \setminus \mathcal{B}_t$
- 15: **end for**
- 16: **return** Final model f_{θ_T}

- **High uncertainty, high misalignment:** Samples at decision boundaries where the model also attends incorrectly ideal for simultaneously improving classification and attention.
- **High uncertainty, low misalignment:** Samples that challenge predictions but with correct attention useful for refining decision boundaries without attention concerns.
- **Low uncertainty, high misalignment:** Confident but attention flawed samples critical for correcting spurious feature dependencies that uncertainty only methods would miss.

Traditional uncertainty-based AL only identifies the first two patterns, systematically overlooking confident-but-wrong-attention samples that are crucial for clinical reliability.

E. Iterative Active Learning Procedure

Algorithm 1 summarizes our complete EG-AL framework. Following the explanation-guided training approach [36], the retraining step uses a composite loss function:

$$\mathcal{L}_{\text{total}} = \mathcal{L}_{\text{cls}} + \alpha \cdot \mathcal{L}_{\text{exp}}, \quad (4)$$

where \mathcal{L}_{cls} is the standard cross-entropy classification loss, \mathcal{L}_{exp} is the Dice loss between Grad-CAM and expert annotations (inversely related to Eq. (2)), and α balances the two objectives, based on validation experiments, we set $\alpha = 0.10$ across all experiments. This ensures that the retrained model not only improves classification but also learns to attend to diagnostically relevant regions, creating a virtuous cycle where better attention improves future sample selection.

IV. EXPERIMENTS

A. Experimental Setup

We evaluate our framework on three expert-annotated medical imaging datasets BraTS [37], VinDr-CXR [38],

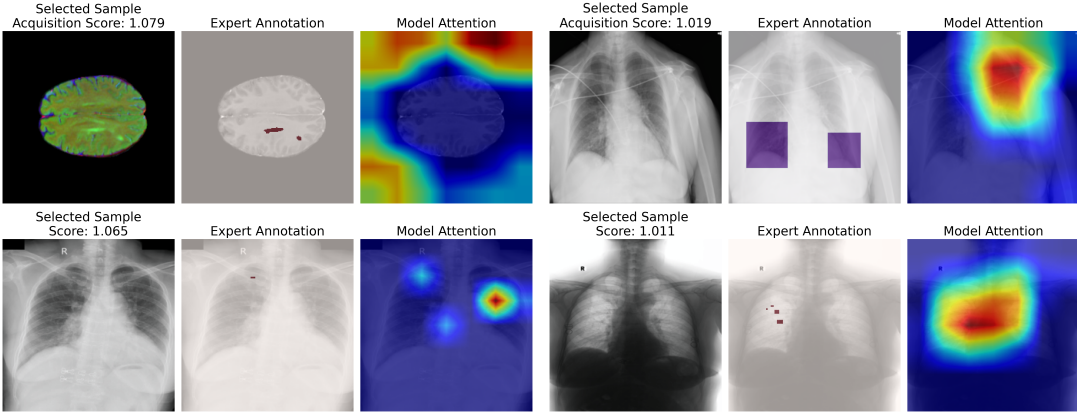


Fig. 3. Representative high-scoring samples selected by EG-AL across different failure patterns. Each example shows: input image with acquisition score, expert annotation, and model attention. Top-left: BraTS case (score 1.079) with small tumor exhibiting high uncertainty and severe attention misalignment. Top-right: VinDr-CXR case (score 1.019) with multiple bounding boxes where model attention scatters across irrelevant regions. Bottom row: Two VinDr-CXR cases showing subtle single opacity (left, score 1.065) and multiple distributed abnormalities (right, score 1.011), both with poor spatial alignment. Our dual-criterion scoring systematically identifies samples where models exhibit classification uncertainty, spatial misalignment, or both.

TABLE I

PERFORMANCE COMPARISON USING 570 TOTAL SAMPLES OVER 7 AL ROUNDS. ACCURACY (%) AND MACRO AUC (%) \pm STD OVER 5 SEEDS.

Dataset	Baseline		Random		EG-AL	
	Acc	Macro AUC	Acc	Macro AUC	Acc	Macro AUC
BraTS	45.10 \pm 1.2	67.52 \pm 1.5	58.01 \pm 3.5	78.32 \pm 2	77.22 \pm 1.4	90.00 \pm 1.1
VinDr-CXR	34.57 \pm 3.2	56.39 \pm 2.8	45.49 \pm 3.5	58.21 \pm 3.1	52.37 \pm 2.4	68.21 \pm 2.9
SIIM-COVID	30.32 \pm 4.1	56.74 \pm 3.7	38.28 \pm 3.8	54.21 \pm 4.2	52.66 \pm 2.7	66.92 \pm 3.3

and SIIM-FISABIO-RSNA-COVID-19 [39] each providing diagnostic labels and spatial annotations for dual-criterion sample selection.

We initialize EG-AL by training a baseline model on 150 randomly selected samples (balanced across classes) using the explainability-guided training objective (Eq. 4) with $\alpha = 0.10$ based on validation experiments. We conduct seven active learning rounds, selecting 60 samples per round based on our composite acquisition score (Eq. 3), resulting in 570 total labeled samples. At each iteration, selected samples are added to the training set and the model is retrained. We compare EG-AL against random sampling under identical conditions.

We use DenseNet-121 [40] pre-trained on ImageNet with a 512-dimensional embedding layer, training via prototypical networks [41] with 5-shot episodes. We set $\lambda = 0.5$ for BraTS and SIIM-COVID, and $\lambda = 0.6$ for VinDr-CXR. All experiments use fixed test sets and report mean accuracy and macro-averaged AUC over 5 random seeds.

B. Performance Comparison

Table I compares EG-AL against baseline and random sampling across all datasets. Our dual-criterion approach consistently achieves superior performance.

For BraTS, EG-AL achieves 77.22% accuracy and 90.00% AUC, outperforming random sampling by 19.21% and 18.68% respectively. The substantial improvement demonstrates that incorporating attention alignment guides models

toward diagnostically relevant tumor boundaries rather than spurious tissue patterns.

On VinDr-CXR, EG-AL reaches 52.37% accuracy and 68.21% AUC, consistently outperforming random sampling across both metrics. Despite the dataset’s complexity with multiple thoracic abnormalities, explanation-guided selection identifies samples that improve spatial reasoning about diagnostically relevant regions.

For SIIM-COVID, EG-AL achieves 52.66% accuracy and 66.92% AUC, substantially exceeding random sampling performance. This validates dual-criterion selection for COVID-19 analysis, where distinguishing severity levels requires precise attention to characteristic lung opacities.

Beyond accuracy improvements, EG-AL demonstrates greater stability across random seeds, with standard deviations consistently lower than random sampling a crucial property for reliable clinical deployment.

C. Sample Selection Analysis

Figure 3 illustrates diverse patterns in EG-AL’s sample selection across three datasets, demonstrating how our dual-criterion approach identifies complementary failure modes. The top-left panel (BraTS, score 1.079) shows a brain tumor case with a small, subtle region where the model exhibits both high classification uncertainty and severe spatial misalignment the attention completely misses the expert-annotated tumor boundary while focusing on surrounding brain tissue.

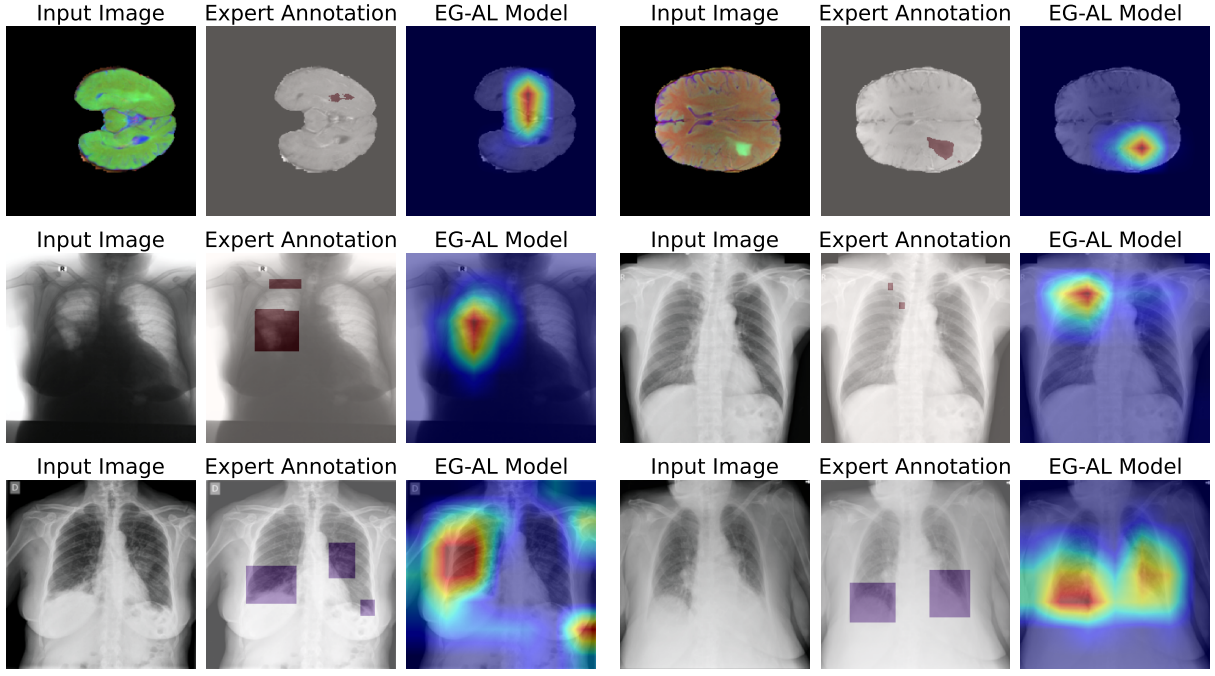


Fig. 4. Attention alignment from models trained with EG-AL-selected samples. Each triplet shows input image, expert annotation, and Grad-CAM (left to right). Top: BraTS tumor cases with small and irregular boundaries. Middle: VinDr-CXR cases with single and multiple thoracic abnormalities. Bottom: SIIM-COVID cases with varying lung opacities. Models consistently localize expert-defined regions regardless of size, number, or complexity, validating that dual-criterion sample selection produces clinically aligned attention.

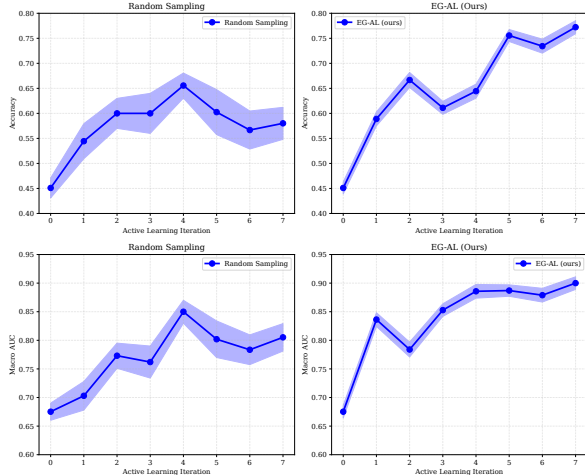


Fig. 5. Progressive performance improvement on BraTS across active learning iterations. Top: Accuracy comparison. Bottom: Macro AUC comparison. Both methods start from the same baseline (iteration 0) and select 60 samples per round. EG-AL demonstrates consistent upward trajectory in both metrics, while random sampling exhibits higher fluctuation in both accuracy (top-left) and macro-auc (bottom-left). Shaded regions indicate standard deviation over 5 random seeds, showing EG-AL’s superior stability.

The top-right panel (SIIM-COVID, score 1.019) exhibits severe attention diffusion across multiple large bounding boxes marking COVID-19 lung opacities. Rather than focusing on the annotated regions, the model’s attention scatters across cardiac structures and background areas, demonstrating confident but fundamentally flawed spatial reasoning.

The bottom row (VinDr-CXR) reveals different failure

patterns in chest radiograph analysis. The bottom-left case (score 1.065) presents a subtle lung abnormality where the model produces weak, diffuse attention that fails to localize the small expert-defined opacity, instead showing scattered focus across the lung field. The bottom-right case (score 1.011) shows a more complex scenario with multiple spatially distributed thoracic abnormalities where the model demonstrates partial attention on some regions while missing others, indicating uncertainty about which features are diagnostically relevant.

These examples validate our core hypothesis: uncertainty-only selection would miss the top-right and bottom-left cases (relatively confident predictions with wrong attention), while explanation-only selection would miss cases with both high uncertainty and misalignment. Our dual-criterion approach systematically identifies both failure modes samples where models struggle with classification AND samples where models predict confidently while attending to incorrect features. This comprehensive coverage ensures selected samples address all pathways to model failure, improving both accuracy and clinical interpretability.

D. Attention Alignment Visualization

Figure 4 demonstrates robust attention alignment from models trained with EG-AL selected samples across diverse diagnostic scenarios. For BraTS (top row), the model accurately localizes tumor boundaries in both small (left) and irregularly shaped (right) cases, focusing precisely on expert-segmented regions rather than surrounding tissue. On VinDr-CXR (middle row), attention correctly highlights thoracic ab-

normalities whether presented as single focal opacities (left) or multiple distributed regions (right), avoiding spurious features like cardiac borders or rib structures. For SIIM-COVID (bottom row), the model consistently identifies characteristic lung opacities aligned with expert bounding boxes across varying opacity patterns and spatial distributions.

These visualizations validate that dual-criterion sample selection produces models with clinically aligned attention regardless of pathology complexity. Models maintain precise spatial focus on small ROIs, correctly prioritize relevant features when multiple abnormalities are present, and accurately localize subtle findings across all datasets. This consistent spatial alignment across challenging cases confirms that our approach fundamentally improves what models learn ensuring attention mechanisms reflect clinical reasoning rather than dataset artifacts or spurious correlations.

E. Active Learning Progression

Figure 5 illustrates the progressive discriminative performance improvement of EG-AL compared to random sampling on BraTS across seven active learning iterations. Starting from identical baselines (45.1% accuracy, 67.5% AUC at iteration 0), both methods iteratively select 60 samples per round.

For accuracy (top), random sampling shows initial improvement but plateaus around 60% with high variance, experiencing performance drops at iterations 5-6. In contrast, EG-AL demonstrates a consistent upward trajectory, achieving 77.2% by iteration 7 a 19.2% absolute improvement over random sampling’s 58.0%.

For Macro AUC (bottom), the pattern is even more pronounced. EG-AL rapidly improves to 90% macro-AUC by iteration 7 with tight confidence bands, while random sampling reaches only 80.5% with significantly higher variance. The AUC progression reveals that EG-AL not only improves accuracy but also produces more confident and well-calibrated predictions across all classes.

The widening performance gap and EG-AL’s consistently tighter variance bands across both metrics validate that our dual-criterion approach systematically identifies samples that enhance both classification performance and model reliability throughout the active learning process. The widening performance gap and EG-AL’s consistently tighter variance bands across both metrics validate that our dual-criterion approach systematically identifies samples that enhance both classification performance and model reliability throughout the active learning process. This sustained improvement demonstrates that explainability-guided selection consistently outperforms random sample acquisition, avoiding the stagnation and high variance observed in random sampling.

F. Impact of Balancing Parameter λ

Figure 6 analyzes the sensitivity of EG-AL to the balancing parameter λ . Peak performance occurs at $\lambda = 0.5$ for BraTS (77.22% accuracy) and SIIM-COVID (52.66% accuracy), and $\lambda = 0.6$ for VinDr-CXR (52.37% accuracy). Critically, both extremes pure uncertainty ($\lambda = 1$) and pure

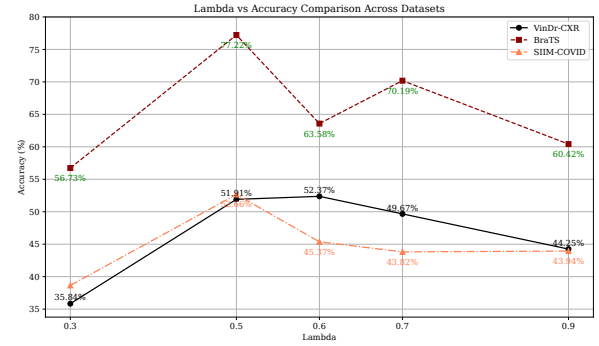


Fig. 6. Effect of λ on EG-AL performance. Optimal values ($\lambda = 0.5$ for BraTS/SIIM-COVID, $\lambda = 0.6$ for VinDr-CXR) demonstrate that balanced consideration of uncertainty and explanation yields superior selection compared to either criterion alone.

explanation ($\lambda = 0$) substantially underperform balanced settings. For BraTS, $\lambda = 0.9$ achieves only $60 \pm 2\%$ while $\lambda = 0.3$ reaches merely $56 \pm 2\%$, representing degradation from optimal respectively. This validates our core hypothesis: effective sample selection requires jointly optimizing what the model doesn’t know (uncertainty) and what it knows incorrectly (attention misalignment). Neither criterion alone suffices for data-efficient learning.

V. CONCLUSION

We presented an explainability-guided active learning framework that combines classification uncertainty with attention-ROI misalignment for sample selection. Our dual-criterion approach systematically identifies samples that improve both predictive accuracy and clinical interpretability, consistently outperforming random sampling across three medical imaging datasets using limited labeled samples. Ablation studies confirm that balanced consideration of uncertainty and explanation yields superior selection compared to either criterion alone. This work establishes interpretability as an integral component of the learning process rather than post-hoc analysis. By integrating clinical knowledge and explanation guidance into sample acquisition, our framework advances toward data-efficient, trustworthy medical AI suitable for clinical deployment. Future work will explore extending the framework to multi-modal settings.

ACKNOWLEDGMENT

This work was supported by the National Science Foundation under Grant No. #2346643, the U.S. Department of Defense under Award No. #FA9550-23-1-0495, and the U.S. Department of Education under Grant No. P116Z240151. Any opinions, findings, conclusions or recommendations expressed in this material are those of the author(s) and do not necessarily reflect the views of the National Science Foundation, the U.S. Department of Defense, or the U.S. Department of Education.

REFERENCES

- [1] K. He, X. Zhang, S. Ren, and J. Sun, “Deep residual learning for image recognition,” in *Proceedings of the IEEE conference on computer vision and pattern recognition*, 2016, pp. 770–778.

[2] J. Chen, Y. Liu, S. Wei, Z. Bian, S. Subramanian, A. Carass, J. L. Prince, and Y. Du, "A survey on deep learning in medical image registration: New technologies, uncertainty, evaluation metrics, and beyond," *Medical Image Analysis*, vol. 100, p. 103385, 2025.

[3] L. Wang and Q. Liang, "Representation learning and nature encoded fusion for heterogeneous sensor networks," *IEEE Access*, vol. 7, pp. 39 227–39 235, 2019.

[4] R. N. Ranabhat, L. Wang, X. Qin, Y. Zhou, and K. Santosh, "Multi-scale unrectified push-pull with channel attention for enhanced corruption robustness," in *Proceedings of the AAAI Symposium Series 2025*, vol. 6, no. 1, 2025, pp. 34–41.

[5] L. Wang, I. I. Uddin, K. Santosh, C. Zhang, X. Qin, and Y. Zhou, "Bridging symmetry and robustness: On the role of equivariance in enhancing adversarial robustness," in *Advances in Neural Information Processing Systems (NeurIPS) 2025*, 2025.

[6] P. Ren, Y. Xiao, X. Chang, P.-Y. Huang, Z. Li, B. B. Gupta, X. Chen, and X. Wang, "A survey of deep active learning," 2021.

[7] H. H. Aghdam, A. Gonzalez-Garcia, J. v. d. Weijer, and A. M. López, "Active learning for deep detection neural networks," in *Proceedings of the IEEE/CVF International Conference on Computer Vision*, 2019, pp. 3672–3680.

[8] K. Wang, D. Zhang, Y. Li, R. Zhang, and L. Lin, "Cost-effective active learning for deep image classification," *IEEE Transactions on Circuits and Systems for Video Technology*, vol. 27, no. 12, pp. 2591–2600, 2017.

[9] L. Wang, P. Chen, C. Wang, and R. Wang, "Layer-wise entropy analysis and visualization of neurons activation," in *International Conference on Communications and Networking in China*. Springer International Publishing Cham, 2019, pp. 29–36.

[10] L. Wang, X. Li, and Z. Zhang, "Dense cross-connected ensemble convolutional neural networks for enhanced model robustness," *arXiv preprint arXiv:2412.07022*, 2024.

[11] N. Nayyem, A. Rakin, and L. Wang, "Bridging interpretability and robustness using lime-guided model refinement," *arXiv preprint arXiv:2412.18952*, 2024.

[12] C. Zhang, D. Gong, and G. Xue, "An uncertainty-incorporated active data diffusion learning framework for few-shot equipment rul prediction," *Reliability Engineering & System Safety*, vol. 254, p. 110632, 2025.

[13] R. R. Selvaraju, M. Cogswell, A. Das, R. Vedantam, D. Parikh, and D. Batra, "Grad-cam: Visual explanations from deep networks via gradient-based localization," pp. 618–626, 2017.

[14] S. M. Lundberg and S.-I. Lee, "A unified approach to interpreting model predictions," *Advances in neural information processing systems*, vol. 30, 2017.

[15] F. Šefčík and W. Benesova, "Improving a neural network model by explanation-guided training for glioma classification based on mri data," *International Journal of Information Technology*, vol. 15, no. 5, pp. 2593–2601, 2023.

[16] A. N. Caragliano, F. Ruffini, C. Greco, E. Ippolito, M. Fiore, C. Tacconi, L. Nibid, G. Perrone, S. Ramella, P. Soda *et al.*, "Doctor-in-the-loop: An explainable, multi-view deep learning framework for predicting pathological response in non-small cell lung cancer," *Image and Vision Computing*, p. 105630, 2025.

[17] J. Sun, S. Lapuschkin, W. Samek, Y. Zhao, N.-M. Cheung, and A. Binder, "Explanation-guided training for cross-domain few-shot classification," in *2020 25th international conference on pattern recognition (ICPR)*. IEEE, 2021, pp. 7609–7616.

[18] C. Wall, L. Wang, R. Rizk, and K. Santosh, "Winsor-cam: Human-tunable visual explanations from deep networks via layer-wise winsorization," *arXiv preprint arXiv:2507.10846*, 2025.

[19] L. Wang, I. I. Uddin, X. Qin, Y. Zhou, and K. Santosh, "Explainability-driven defense: grad-cam-guided model refinement against adversarial threats," in *Proceedings of the AAAI Symposium Series (AAAI) 2025*, vol. 6, no. 1, 2025, pp. 49–57.

[20] W.-N. Hsu and H.-T. Lin, "Active learning by learning," in *Proceedings of the AAAI Conference on Artificial Intelligence*, vol. 29, no. 1, 2015.

[21] S. Ho, M. Liu, S. Gao, and L. Gao, "Learning to learn for few-shot continual active learning," *Artificial Intelligence Review*, vol. 57, no. 10, p. 280, 2024.

[22] S. Ravi and H. Larochelle, "Optimization as a model for few-shot learning," in *International conference on learning representations*, 2017.

[23] A. Biswas, N. M. Abdullah Al, M. S. Ali, I. Hossain, M. A. Ullah, and S. Talukder, "Active learning on medical image," in *Data Driven Approaches on Medical Imaging*. Springer, 2023, pp. 51–67.

[24] M. Gaillochet, C. Desrosiers, and H. Lombaert, "Active learning for medical image segmentation with stochastic batches," *Medical Image Analysis*, vol. 90, p. 102958, 2023.

[25] Z. Zhou, J. Y. Shin, S. R. Gurudu, M. B. Gotway, and J. Liang, "Active, continual fine tuning of convolutional neural networks for reducing annotation efforts," *Medical image analysis*, vol. 71, p. 101997, 2021.

[26] H. Zhan and N.-C. Xiao, "A new active learning surrogate model for time-and space-dependent system reliability analysis," *Reliability Engineering & System Safety*, vol. 253, p. 110536, 2025.

[27] R. Hao, K. Namdar, L. Liu, and F. Khalvati, "A transfer learning-based active learning framework for brain tumor classification," *Frontiers in artificial intelligence*, vol. 4, p. 635766, 2021.

[28] L. Wang, C. Wang, Y. Li, and R. Wang, "Explaining the behavior of neuron activations in deep neural networks," *Ad Hoc Networks*, vol. 111, p. 102346, 2021.

[29] M. Shi, R. Wang, E. Liu, Z. Xu, and L. Wang, "Deep reinforcement learning based computation offloading for mobility-aware edge computing," in *International conference on communications and networking in china*. Springer International Publishing Cham, 2019, pp. 53–65.

[30] L. Wang, C. Wang, Y. Li, and R. Wang, "Improving robustness of deep neural networks via large-difference transformation," *Neurocomputing*, vol. 450, pp. 411–419, 2021.

[31] K. Xiao, L. Wang, A. Gupta, and X. Qin, "Looking beyond content: Modeling and detection of fake news from a social context perspective," in *HICSS*, 2022, pp. 1–10.

[32] H. W. Loh, C. P. Ooi, S. Seoni, P. D. Barua, F. Molinari, and U. R. Acharya, "Application of explainable artificial intelligence for healthcare: A systematic review of the last decade (2011–2022)," *Computer methods and programs in biomedicine*, vol. 226, p. 107161, 2022.

[33] Z. Sadeghi, R. Alizadehsani, M. A. Cifci, S. Kausar, R. Rehman, P. Mahanta, P. K. Bora, A. Almasri, R. S. Alkhawaldeh, S. Hussain *et al.*, "A review of explainable artificial intelligence in healthcare," *Computers and Electrical Engineering*, vol. 118, p. 109370, 2024.

[34] L. Wang, W. Chen, and J. Li, "Congestion aware dynamic user association in heterogeneous cellular network: A stochastic decision approach," in *2014 IEEE International Conference on Communications (ICC)*. IEEE, 2014, pp. 2636–2640.

[35] L. Wang, A. Ghimire, K. Santosh, Z. Zhang, and X. Li, "Enhanced robustness by symmetry enforcement," in *IEEE Conference on Artificial Intelligence (IEEE CAI) 2024*, 2024.

[36] I. I. Uddin, L. Wang, and K. Santosh, "Expert-guided explainable few-shot learning for medical image diagnosis," in *Data Engineering in Medical Imaging: Third MICCAI Workshop, DEMI 2025, Held in Conjunction with MICCAI 2025, Daejeon, South Korea, September 27, 2025, Proceedings*. Springer Nature, 2025, p. 95.

[37] B. H. Menze, A. Jakab, S. Bauer, J. Kalpathy-Cramer, K. Farahani, J. Kirby, Y. Burren, N. Porz, J. Slotboom, R. Wiest *et al.*, "The multimodal brain tumor image segmentation benchmark (brats)," *IEEE transactions on medical imaging*, vol. 34, no. 10, pp. 1993–2024, 2014.

[38] H. Q. Nguyen, K. Lam, L. T. Le, H. H. Pham, D. Q. Tran, D. B. Nguyen, D. D. Le, C. M. Pham, H. T. Tong, D. H. Dinh *et al.*, "Vindr-cxr: An open dataset of chest x-rays with radiologist's annotations," *Scientific Data*, vol. 9, no. 1, p. 429, 2022.

[39] P. Lakhani, J. Mongan, C. Singhal, Q. Zhou, K. P. Andriole, W. F. Auffermann, P. Prasanna, T. Pham, M. Peterson, P. J. Bergquist, T. S. Cook, S. F. Ferracioli, G. C. de Antonio Corradi, M. Takahashi, S. S. Workman, M. Parekh, S. Kamel, J. H. Galant, A. Mas-Sanchez, E. C. Benítez, M. Sánchez-Valverde, L. Jaques, M. Panadero, M. Vidal, M. Culiáñez-Casas, D. M. Angulo-Gonzalez, S. G. Langer, M. de la Iglesia Vaya, and G. Shih, "The 2021 siim-fisabio-rsna machine learning covid-19 challenge: Annotation and standard exam classification of covid-19 chest radiographs," *OSF Preprints*, October 21 2021.

[40] G. Huang, Z. Liu, L. Van Der Maaten, and K. Q. Weinberger, "Densely connected convolutional networks," in *Proceedings of the IEEE conference on computer vision and pattern recognition*, 2017, pp. 4700–4708.

[41] J. Snell, K. Swersky, and R. Zemel, "Prototypical networks for few-shot learning," *Advances in neural information processing systems*, vol. 30, 2017.